Catalysis Letters (2019) 149:723–732
https://doi.org/10.1007/s10562-018-02649-8

Preparation of Betulone Via Betulin Oxidation Over Ru Nanoparticles Deposited on Graphitic Carbon Nitride

N. D. Shcherban[1,2] · P. Mäki-Arvela[2] · A. Aho[2] · S. A. Sergiienko[3] · M. A. Skoryk[4,5] · E. Kolobova[6] · I. L. Simakova[7] · K. Eränen[2] · A. Smeds[2] · J. Hemming[2] · D. Yu. Murzin[2]

Received: 5 July 2018 / Accepted: 9 December 2018 / Published online: 17 January 2019
© The Author(s) 2019

Abstract

Derivatives of betulin obtained by oxidation have broad pharmacological applications, demonstrating anti-inflammatory, antioxidant, hepatoprotective, and anticancer activity. Ru supported catalysts based on graphitic carbon nitride or N-doped carbon were prepared via a mild reduction of the initial Ru precursor with hydrazine. These catalysts along with Ru supported on carbon nanofibers and a mesoporous carbon support Sibunit were studied in catalytic oxidation of betulin. Ru/carbon nitride demonstrated catalytic activity in betulin oxidation higher than Ru/N-doped carbon (conversion of betulin up to ca. 70% and 30%, respectively). Selectivity to different oxidation products was dependent on the properties of the carbon supports.

Graphical Abstract

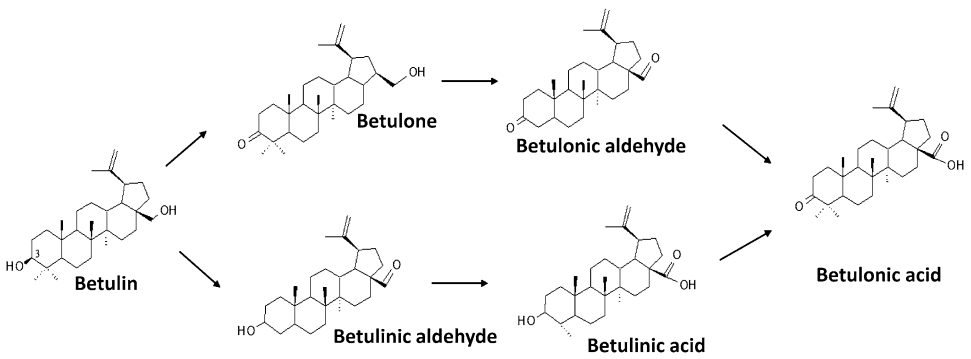

Keywords Betulin oxidation · Carbon nitride · Ruthenium · Betulone

Electronic supplementary material The online version of this article (https://doi.org/10.1007/s10562-018-02649-8) contains supplementary material, which is available to authorized users.

✉ D. Yu. Murzin
dmurzin@abo.fi

[1] L.V. Pisarzhevsky Institute of Physical Chemistry, National Academy of Sciences of Ukraine, 31 pr. Nauky, Kiev 03028, Ukraine

[2] Johan Gadolin Process Chemistry Centre, Åbo Akademi University, Biskopsgatan 8, 20500 Åbo/Turku, Finland

[3] National University of Science and Technology MISiS, Leninskii pr. 4, 119049 Moscow, Russia

[4] NanoMedTech LLC, 68 Gorkogo str., Kiev, Ukraine

[5] G.V. Kurdyumov Institute for Metal Physics, N.A.S. of Ukraine, 36 Academician Vernadskiy av., Kiev 03680, Ukraine

[6] Research School of Chemistry & Applied Biomedical Sciences, Tomsk Polytechnic University, Lenin Avenue 30, Tomsk 634050, Russia

[7] Boreskov Institute of Catalysis, Lavrentieva ave. 5, Novosibirsk, Russia

1 Introduction

Betulin is a natural compound from a class of lupane-type pentacyclic triterpenes possessing interesting biological properties [1–3]. Betulin derivatives obtained by oxidation (Fig. 1) have a wide spectrum of pharmacological action, which include anti-inflammatory, antioxidant, hepatoprotective, anticancer and other ones [4–10]. Lupane-type compounds have antitumor activity, among them the strongest effect is belonging to betulinic acid, which is recognized as an effective inhibitor of the growth of cancer cells [11]. Betulin, betulinic acid and betulonic acid are also interesting from the medical point of view as a basis for creation of new antiviral medicines showing inhibitory effect. Allobetulin has a moderately expressed effect on the influenza virus type B [12].

Betulonic acid is prepared via betulin oxidation in acetone with the Jones reagent [13–15]. This compound can also be obtained as a result of betulin oxidation with a pyridine-dichromate complex with acetic anhydride in dimethylformamide [16] and chromium (VI) oxide in acetic acid [17].

Betulinic aldehyde is formed as a result of betulin oxidation with potassium dichromate on silica gel in dichloromethane [18]. Reaction between betulin and chlorochromate or pyridinium dichromate in dichloromethane leads to formation of betulonic aldehyde [19]. Synthesis of betulinic acid consists of reduction of betulonic acid with sodium borohydride [15] (Fig. 1). For oxidation of betulin to betulinic acid with iodine or (diacetoxyodo)benzene as oxidants, TEMPO (2,2,6,6-tetramethylpiperidine oxyl) as a catalyst was also used [20]. When $RuCl_2(PPh_3)_3$ as a homogeneous catalyst and TEMPO as a co-catalyst were also used for betulin oxidation in oxygen, the yields of betulinic aldehyde at 1 bar and 105 °C and 8 bar and 100 °C were 15% (27 h) and 69% (8 h), respectively [21].

Use of Ru/C as a catalyst in a mixture with the basic hydrotalcite and silicon dioxide as a dehydrating agent allowed to perform selective oxidation of betulin with synthetic air at 108 °C in toluene to betulinic aldehyde [5]. The presence of silica in the reaction mixture leads to a significant increase in the betulin conversion (41% and 20%, respectively, after 24 h) with similar selectivity (67% and 66%, respectively). The use of ruthenium nanoparticles deposited on an acidic carbon support results in the formation of allobetulin as the main reaction product [5].

Another betulin derivative, betulone, is present in quite low quantities in many plants [22, 23]. Regarding its biological activity it was noted that selective oxidation of 3-hydroxyl group in the initial compound results in a significant increase in biological activity compared with betulin (regulation of melanin biosynthesis, anticancer activity etc.) [24, 25]. Moreover, betulone can be used as the main building block for the synthesis of another valuable product allobetulone [26]. Betulone was prepared from betulin through regioselective oxidation using growing microorganism cells as catalyst [1].

Graphitic carbon nitride possessing besides interesting electronic properties also catalytic activity due to the presence of Lewis basic sites [27] seems to be a suitable support for preparation of catalysts active in betulin oxidation. The number of publications devoted to investigations of catalytic performance of Ru nanoparticles supported on graphitic C_3N_4 is rather limited. For instance, Ru/g-C_3N_4 demonstrated promising catalytic activity and a high turnover frequency number in the hydrolysis of ammonia borane which provides an eco-friendly and sustainable way to hydrogen production [28]. Deposition of Pt_{50}–Ru_{50} alloy catalyst on nanoporous graphitic C_3N_4 as a support allowed to increase the anodic performance in direct methanol fuel cells due to well-developed three-dimensionally interconnected porosity of the support [29].

The aim of the current study was to investigate betulin oxidation over ruthenium nanoparticles supported on graphitic carbon nitride. For comparison, nitrogen-containing carbon and several undoped carbons were also used as supports.

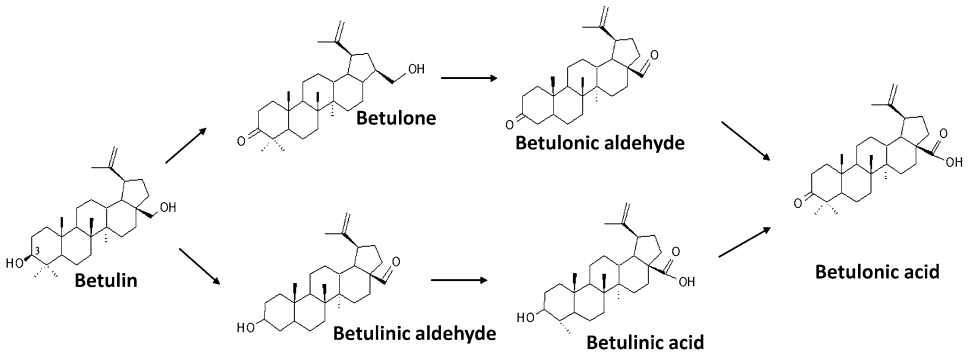

Fig. 1 Scheme of betulin oxidation

2 Experimental

2.1 Sample Preparation

Initial samples of nanostructured graphitic carbon nitride and N-doped carbon were obtained by bulk and hard template method using melamine, as well as sucrose and melamine as precursors, respectively.

The material denoted as C_3N_4–1 was prepared via bulk pyrolysis of melamine (Chimlaborreactiv, 99%). For this purpose melamine was placed in the middle of the quartz tube, followed by heating in an inert atmosphere (argon) at 500 °C for 2 h. As a result yellow carbon nitride powder was obtained. C_3N_4–2 was synthesized using a similar technique, except that the heat treatment was carried out in air. For synthesis of C_3N_4–MCF a weighed amount of MCF mesoporous silica was mixed with an aqueous solution containing a certain amount of melamine and hydrochloric acid (Lachema, 35%) used for melamine binding into the salt in order to reduce its sublimation (ca. 2.356 g of melamine and 1.8 ml of concentrated hydrochloric acid for 0.5 g of MCF). The resulting suspension was stirred on a magnetic stirrer at a room temperature for 3 h and dried at 40 °C for 12 h. The obtained composite was then subjected to heat treatment in argon at 600 °C for 2 h. For a more complete filling of the hard template pores with the substance after pyrolysis a second impregnation step of the composite with melamine was performed using the same procedure. The silica component was removed by treatment of the obtained composites with 15% HF (Merck, 40%) solution for 12 h. Carbon nitride was filtered and washed to a neutral pH value, and then dried at 100 °C. For synthesis of N-doped carbon (C_M sample) the product of bulk carbonization of sucrose at 900 °C for 2.5 h was used as the initial material. For doping of the carbon structure with nitrogen 3 g of the obtained carbon was treated with ethanol solution of melamine (2 g of melamine in 10 mL of ethanol) and stirred at a room temperature for 5 h. The obtained suspension was boiled in order to evaporate alcohol and then the mixture was dried at 120 °C. The impregnated carbon was heated in argon atmosphere up to 950 °C (heating rate 10 °C/min) and kept at this temperature for 0.5 h. Then the sample was washed with hot distilled water to neutral pH of wash water in order to remove any excess of melamine decomposition products.

In order to avoid significant changes in the chemical nature of the support surface, ruthenium nanoparticles were deposited using a mild reduction of the initial Ru precursor with a chemical reducing agent (hydrazine) similar to an approach described in [30]. A weighted amount of ruthenium trichloride (0.0409 g) (Merck, 99.98%), based on the content in the composite of 5 wt%, was dissolved in 250 ml of deionized water. The support sample (0.3 g) was added to the resulting solution and stirred at a room temperature for ca. 16 h. After water evaporation the residue was dried at 120 °C for 3 h. The resulting sample was stirred in 100 ml of 0.1 M KOH (Merck, 85%) solution at a room temperature for 10 min, thereafter hydrazine (Merck, 80%) was added (molar ratio of hydrazine:ruthenium was 2), slowly heated up to 80 °C, and maintained at this temperature for 1 h. The sample was filtered, washed with distilled water to a neutral pH of wash water and dried at 100 °C.

Two Ru catalysts were synthesized using different undoped carbons: carbon nanofibers of the platelet structure (CNF-Pl) (fraction 50-120m, FutureCarbon GmbH, R141402333-01) and a mesoporous carbon material Sibunit (fraction 50-120m). The catalyst denoted as Ru-CNF (2 wt% Ru) was prepared by immobilization on CNF-Pl colloidal Ru nanoparticles (0.1 M) synthesized by the polyol method using $RuCl_3 \cdot nH_2O$ and ethylene glycol (EG) as a metal precursor and a reducing agent, respectively, and polyvinylpyrrolidone (PVP) as a stabilizing agent. As a general procedure, $RuCl_3 \cdot nH_2O$ and PVP (mol Ru/mol monomers PVP = 1/5) were dissolved in EG under stirring followed by heating up to 198 °C for 1 h. Ru nanoparticles supported on CNF-Pl were subjected to thermal treatment in air at 180 °C with a temperature ramp 10 K/min during 0.5 h followed by reduction in hydrogen at 250 °C with temperature ramp 1.5 K/min during 1 h to remove excess of PVP [31]. The catalyst denoted as Ru-Sib-Imp (3 wt%) was prepared by impregnation of Sibunit with $RuCl_3 \times nH_2O$ aqueous solution (0.1 M) [32] followed by oxidation in air at 150 °C during 1.5 h and reduction in hydrogen until 440 °C during 6 h with temperature ramp 10 K/min. The metal loading in those catalysts was measured by XRF.

2.2 Characterization

Phase composition of the samples was analyzed using Bruker D8 Advance diffractometer equipped with Cu K_α ($\lambda = 0.15406$ nm) X-ray source, in the range of $2\theta = 3°$–$60°$ at a scan rate of 1 deg/min.

Morphology of the samples was investigated using scanning electron microscopy (SEM) with MIRA3 TESCAN microscope at accelerating voltage of 5–20 kV.

TEM images were obtained using the field emission TEM JEM-2100 (JEOL) with an accelerating voltage of 100 kV. The samples for TEM were ground in agate mortar with ethanol, and then the suspension was deposited on a copper grid coated with a carbon film.

Porous texture characterization of the carbon nitride and carbon samples was carried out by nitrogen physisorption at − 196 °C using Sorptomatic 1990 after outgassing the samples at 200 °C under vacuum for 4 h. The total surface area,

S_{BET}, was calculated using the BET equation [33]. Mesopore size was determined using the Barrett–Joyner–Halenda method from the desorption branch of the isotherm [34]. The micropore size was calculated according to the Horvath–Kawazoe equation [35].

XPS-analysis of the samples was made using Perkin-Elmer PHI 5400 spectrometer with a Mg K_α X-ray source operated at 14 kV and 200 W. The samples were kept in the preparation chamber of the XPS equipment overnight before analysis. The pass energy of the analyzer was 17.9 eV and the energy step 0.1 eV. The charging was adjusted according to the C–C bond at 284.5 eV. Peak fitting was performed with the program XPS Peak 4.1. The background was corrected with the Shirley function.

Semi-quantitative analysis of metal concentrations was performed using wavelength dispersive X-ray fluorescence (WDXRF) spectrometry with the powder pellet method. Undiluted samples (0.5 g) were milled and put in the 29 mm diameter die. The intensities of the metal lines in the samples were measured in vacuum conditions on an ARL Advant'X spectrometer equipped with a rhodium anode X-Ray tube. Excitation conditions were as follows: tube voltage of 50 kV; current of 40 mA; collimator with a divergence of 0.25°; LiF200 crystal was used as a monochromator; scintillation counter was used as a detector; counting time was 12 s. The content of elements in the sample was estimated using a semi-quantitative method by means of a QuantAS program for standard-less analysis.

The basicity of the tested materials was determined by temperature programmed desorption of CO_2 using a Micromeritics Autochem 2910 equipment. Prior to adsorption of CO_2 a sample was heated to 400 °C (10 °C/min) in a 10 ml/min flow of helium and kept at this temperature for 60 min. Thereafter, the sample was cooled to ambient temperature and CO_2 was adsorbed to the catalyst for 30 min with a 50 ml/min flow. After CO_2 adsorption the sample was flushed with helium (20 ml/min) for 30 min to remove physisorbed CO_2. The temperature programmed desorption was carried out with a 10 °C/min heating rate until 600 °C, the TCD signal was recorded every second.

2.3 Catalytic Tests

Betulin (90–94% purity) was extracted from birch with a nonpolar solvent and recrystallised from 2-propanol following the literature procedure [36]. Betulin oxidation was performed over synthesized Ru catalysts at a temperature of 140 °C and atmospheric pressure using a batch-mode operated glass reactor. Synthetic air (AGA, 20% oxygen, 80% nitrogen) was used as an oxidant, mesitylene—as a solvent. In a typical catalytic experiment, betulin oxidation was carried out using 200 mg of reagent in 100 ml of solvent, as well as 200 mg of catalyst. Before the reaction, the catalyst was heated to 200 °C in an argon atmosphere for 60 min.

The samples were taken at different time intervals. Before analysis of the samples by gas chromatography (GC), a sample of 0.5 ml was silylated using *N,O*-Bis(trimethylsilyl) trifluoroacetamide, BSTFA (Acros, > 98%), 100 µl, and trimethylchlorosilane, TMCS (Fluka, > 99%), 25 µl, and pyridine (VWR Chemicals, > 99%) 25 µl, respectively, at 70 °C for 1 h. The silylated reaction mixtures were analyzed with a gas chromatograph using HP-1 column (25 m, 200 µm, 0.11 µm) applying the following temperature program: 120 °C (1 min)—6 °C/min—320 °C (15 min) and a split ratio of 25:1. The injector temperature was 260 °C and the detector temperature was 320 °C. The products were confirmed by GC–MS using HP-5 column.

3 Results and Discussion

Pyrolysis of melamine leads to the formation of structures with high-angle peaks (2θ ~ 27.3–27.7°) on the X-ray diffraction patterns (Fig. 2) corresponding to the average interlayer distance of d = 0.327–0.322 nm similar to the (002) plane of graphitic carbon nitride. The average crystallite sizes calculated according to the broadening of (002) peak by the Scherrer's formula [37] are ca. 6–7 nm. Synthesized carbon, doped with nitrogen (C_M), is an amorphous material because the corresponding X-ray diffraction pattern does not contain any reflexes, including those ones characteristic for the graphite structure.

According to SEM-images (Fig. 3a) carbon nitride obtained by bulk pyrolysis consists of relatively large monolithic particles (from 200 nm to a few microns). Carbon nitride prepared using silica template (C_3N_4–MCF) is

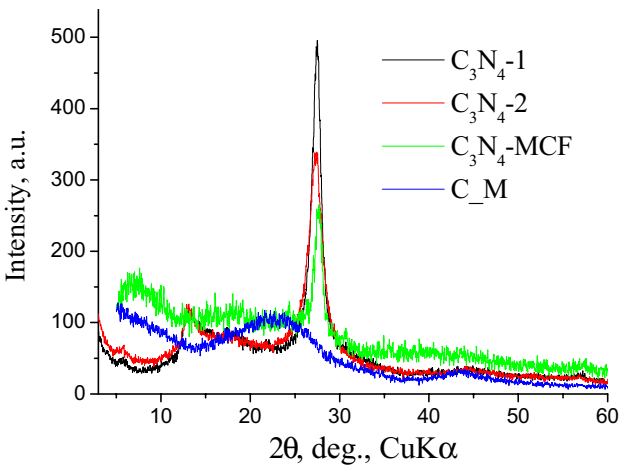

Fig. 2 X-ray diffraction patterns of the obtained carbon nitride and nitrogen-doped carbon samples

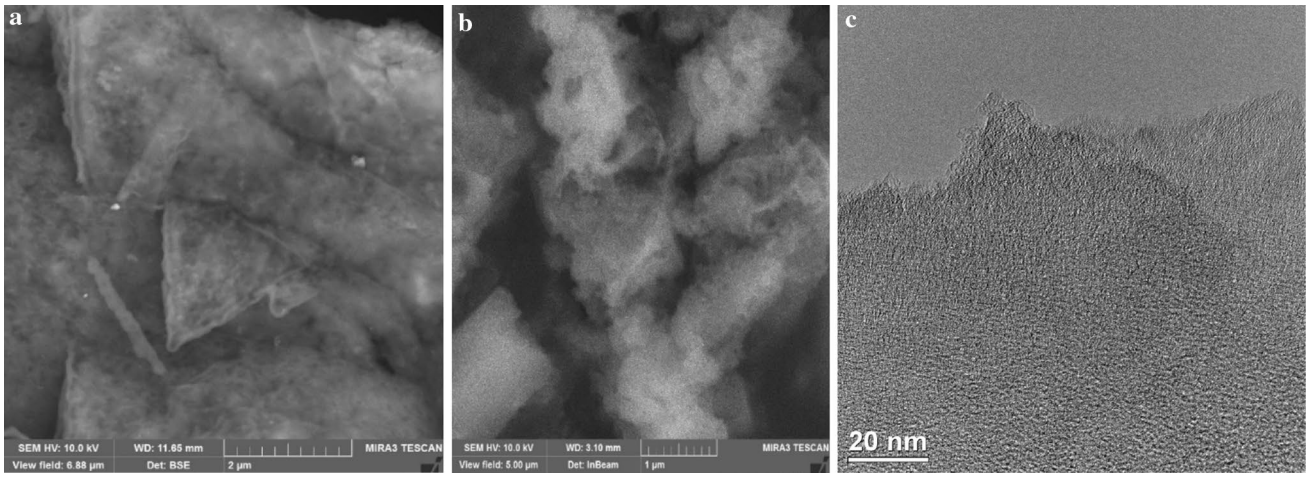

Fig. 3 SEM- and TEM-images of the obtained samples: SEM: **a** C_3N_4–1, **b** C_3N_4–MCF; TEM: **c** C_M

characterized by a more friable structure (Fig. 3b). Such slightly more developed structure apparently can be due to the presence of silica acting as a template during the thermal treatment. N-doped carbon (C_M) is characterized by a well-developed structure possessing slit-like micropores with a size of ca. 0.5 nm (Fig. 3c).

The textural characteristics of the prepared carbon nitride and N-doped carbon calculated from nitrogen adsorption–desorption isotherms are presented in Table 1. C_3N_4–1 and C_3N_4–2 contain large mesopores (D_{meso} 40–50 nm). C_3N_4–MCF possesses smaller mesopores (D_{meso} ca. 30 nm) which can be associated with the presence of the template in comparison with carbon nitride prepared via traditional melamine bulk pyrolysis.

Application of silica template (mesoporous cellular foam MCF) results in some increase of carbon nitride porosity, in particular BET specific surface area (22 m^2/g) and pore volume (0.16 cm^3/g) compared to typical C_3N_4 (10 m^2/g and 0.04 cm^3/g, respectively, Table 1). Completely mesoporous structures (without micropores) of the prepared carbon nitride samples should be noted.

N-doped carbon (C_M) is a homogeneously microporous material with the micropore volume of 0.17 cm^3/g. Micropores ($D_{micro} \leq 1$ nm) constitute 85% of the total pore volume testifying a high uniformity of microporous structure in the obtained sample (Table 1).

Temperature-programmed desorption curves of carbon dioxide (TPD CO_2) from synthesized g-C_3N_4 and nitrogen-doped carbon samples contain one main maximum of carbon dioxide desorption at ca. 130–160 °C (Fig. 4a). Deconvolution of the indicated curves (Fig. 7 b) using the Gaussian distribution function gives two main peaks with the temperature maxima of carbon dioxide desorption at ca. 90–100 °C and 130–160 °C, which can be attributed to physisorption and adsorption of CO_2 on weak basic sites, respectively. The corresponding concentrations of the basic sites without taking into account the physically adsorbed carbon dioxide are ca. 40–80 µmol/g (shoulder with the CO_2 desorption maximum at 130–160 °C).

Deposition of ruthenium trichloride followed by reduction leads to formation of ruthenium nanoparticles with a diameter ranging from 1 to 5 nm (Fig. 5) which is close to the particle sizes obtained in [32]. It should be noted that carbon nitride contributes to the formation of relatively homogeneous nanoparticles (maxima of particle size distribution are 1.7, 1.3, 4.0 and 1.6 nm for Ru–C_3N_4–1, Ru–C_3N_4–2, Ru–C_3N_4–MCF and Ru–C_M, respectively, Fig. 5), which can be connected with stabilizing effect of the carbon nitride surface [38]. The average particle sizes

Table 1 Structural-sorption characteristics of supports (N_2, 77 K)

Sample	V_{micro}, cm^3/g	V_{meso}, cm^3/g	D_{meso}, nm	S_{meso}, m^2/g	S_{BET}, m^2/g	V_{ads}, cm^3/g
C_3N_4–1	0.003	0.04	38	10	10	0.04
C_3N_4–2	–	0.06	~50	10	10	0.06
C_3N_4–MCF	–	0.16	33	19	22	0.16
C_M	0.17	–	–	–	630	0.20
Sibunit					350	0.56
CNF-PI					123	0.29

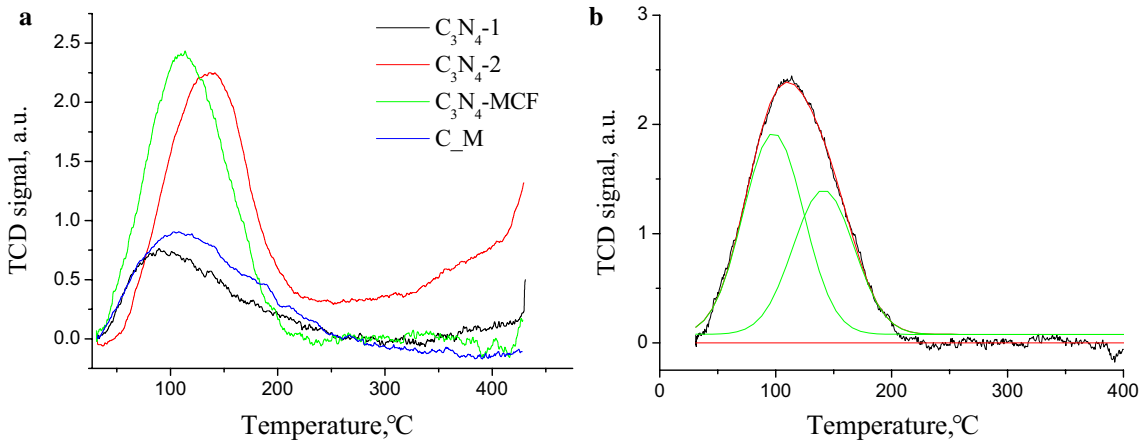

Fig. 4 CO_2-TPD profiles for the prepared carbon nitride and carbon samples (**a**) and deconvolution for C_3N_4–MCF (**b**)

for Ru-CNF and Ru-Sib-Imp catalysts were 2.5 and 1.3 nm respectively.

The chemical state of Ru in the obtained composites was characterized by XPS (Fig. 6). Ru 3d XPS spectra (Fig. 6 a, b) consist of two main peaks at binding energies 280.7 and 280.2 eV assigned to Ru (4+) of the ruthenium oxide (RuO_2) and the Ru (0) metal peak, respectively [39, 40]. Formed Ru particles being quite small (mainly 2–4 nm) are exposed to surface oxidation, therefore resulting in the formation of a core–shell structures [39]. In fact a high content of Ru in a high oxidation state is observed even in classical Ru/C catalysts and Ru/CNT after hydrogenation of sugars [41, 42]. Other peaks belong to C 1 s region of the support. In particular, two main peaks at 284.5 and 287.9 eV (Fig. 6a, b) correspond to sp^2 C–C bonds and sp^2-bonded carbon in N-containing aromatic rings (N–C=N) [43]. Ru 3p XPS spectra, compared to Ru 3d spectra, do not overlap with other signals allowing monitoring the oxidation state (Fig. 6c, d). These spectra can be deconvoluted into three peaks. The peak at a binding energy of 461.2 eV can be attributed to Ru (0) from metal atoms, at 463.0–463.5 eV to RuO_2 and at 465.8–466.3 eV to RuO_x [39, 40].

Catalytic activity of Ru supported catalysts based on the graphitic carbon nitride and N-doped carbon was tested in the betulin oxidation with synthetic air. In order to compare the influence of the support nature and porosity, Ru catalysts supported on different undoped carbons (mesoporous Sibunit and carbon nanofibers) were also investigated.

Ru/carbon nitride possesses catalytic activity in betulin oxidation higher than Ru/N-doped carbon (ca. 70% and 30% conversion of betulin, respectively, Table 2). Probably, it can be due to several reasons: (1) a significant fraction of defects serving as active sites as well as presence of weak Lewis basic sites on the surface of carbon nitride, (2) better dispersion of the Ru nanoparticles and (3) more effective mass transfer compared to only microporous Ru/N-doped carbon. Betulone was the main desired product over the studied catalysts (selectivity up to 27%). The mass spectrum of betulone is presented in SI. The peaks of by-products in GC–MS are very small and therefore their identification is very challenging. In general, by-products were represented by several esters/ethers. Utilization of Ru-CNF prepared by the colloidal method resulted in a much less active catalyst forming mainly betulone (33% selectivity) while Ru-Sib-Imp afforded higher conversion that Ru-CNF not, however, comparable with Ru/carbon nitride catalysts. Selectivity to betulinic aldehyde was at the same time the highest (ca. 15%) especially considering that conversion was lower for Ru-Sib-Imp than in the case of Ru–C_3N_4 (Table 2).

Typical kinetic plots showing the main identified components in the reaction mixture are presented in Fig. 7. As can be seen from the kinetic curves Ru–C_3N_4–MCF allows achieving a more rapid betulin transformation and formation of the reaction products (betulone, betulonic aldehyde, betulonic acid, betulinic aldehyde, betulinic acid, lupeol) in higher concentrations than Ru deposited on N-doped carbon and undoped carbons. However faster formation of other (unidentified) products should be noted which can be due to an overall higher catalytic activity of Ru–C_3N_4–MCF resulting in generation of side products together with the desired ones. Application of Ru nanoparticles supported on a conventional carbon support (Ru/C, Degussa) as a catalyst results in a predominant formation of allobetulin (selectivity 72%, conversion 54%) which was assigned to acidic sites inherent to the support [5]. Use of basic supports (i.e. carbon nitride and N-doped carbon) allows avoiding allobetulin generation and it can be possibly responsible for higher oxidation activity involving basic sites. Better catalytic performance of Ru–C_3N_4–MCF in comparison with Ru-C_3N_4–1 and Ru–C_3N_4–2 manifested in increased selectivity toward the desired products (Table 2) can be associated with a better developed porosity (Table 1) and reticulated structure

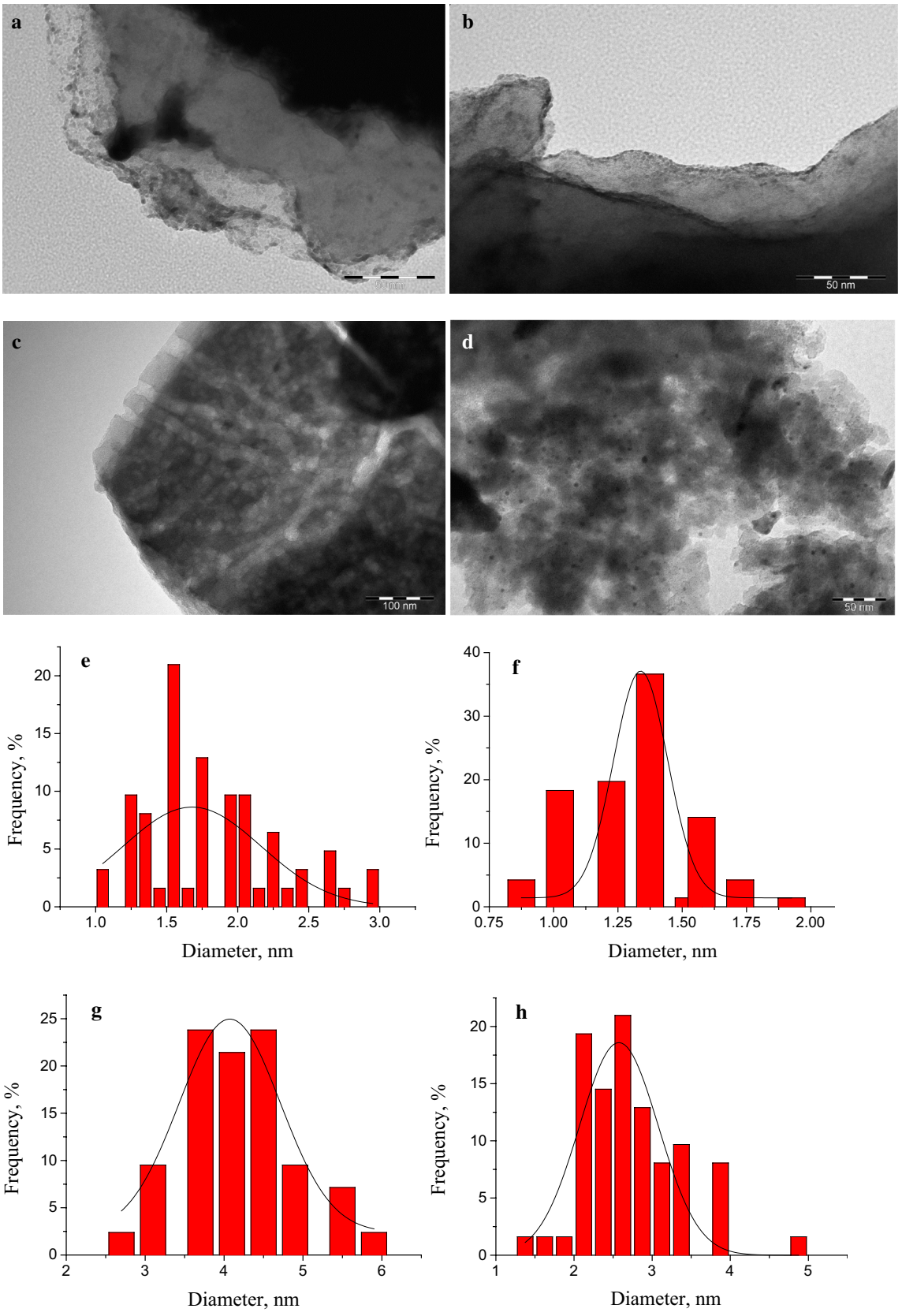

Fig. 5 TEM-images and particle size distributions for the composites based on graphitic carbon nitride or nitrogen-doped carbon with ruthenium nanoparticles: **a, e** Ru–C_3N_4–1, **b, f** Ru–C_3N_4–2, **c, g** Ru–C_3N_4–MCF, **d, h** Ru–C_M

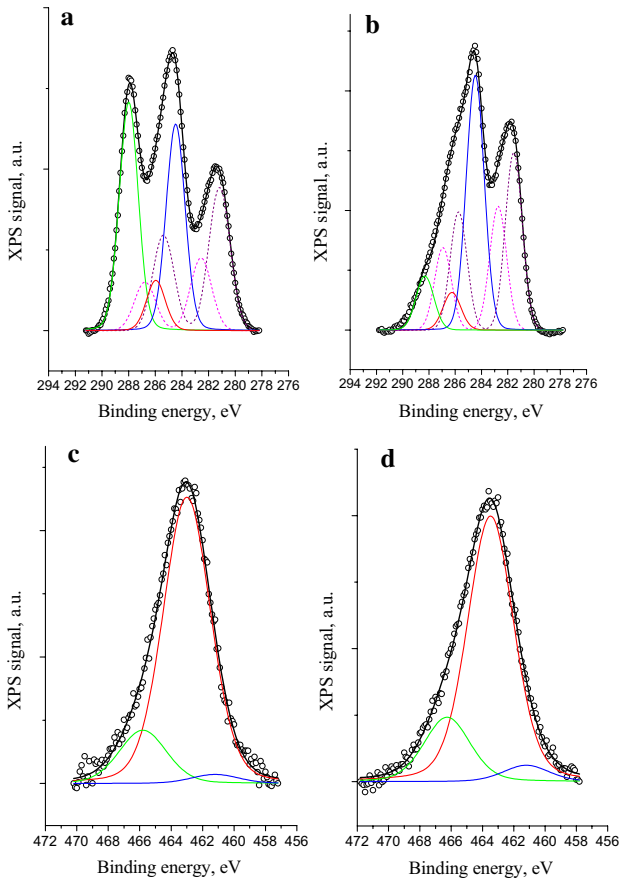

Fig. 6 XPS spectra of Ru 3d (**a, b**) and Ru 3p (**c, d**) regions for Ru–C_3N_4–2 (**a, c**) and Ru–C_M (**b, d**)

(Fig. 4c) of Ru–C_3N_4–MCF obtained via the hard-templating method.

Selectivity towards betulone as a function of betulin conversion presented in Fig. 8, contains maxima, testifying probably intensification of the side products formation.

Comparing the catalytic results it can be suggested that the presence of weak basic sites in the structure of the support (carbon nitride and N-doped carbon) increases the betulin conversion, while application of the carbon supports with a developed porosity (Ru-Sib-Imp) leads to an increase of selectivity not only towards betulone, but also towards another important product—betulinic aldehyde (Table 2).

There are available data in the literature on the preparation of betulone from betulin using microorganisms. For example, the yield of betulone was up to 25% at 33 °C after 6 days [1]. Data on the preparation of betulone from betulin using heterogeneous catalysts according to our knowledge are absent. The maximal yield of betulone achieved in the current study is ca. 14% after 3 h using Ru–C_3N_4–MCF as the catalyst. The obtained data can be used for further investigation and improvement of the catalytic performance of Ru supported heterogeneous catalysts in betulin oxidation to useful pharmaceutical products including betulone.

It should be noted that, as a result of catalytic experiments, the reaction mixture became yellow, which according to GC–MS data was due to partial oxidation of the solvent (mesitylene) to 3,5-dimethylbenzoic acid.

High oxidative activity of the prepared materials and formation of betulone can be associated with the presence of RuO_2 in the nanoparticles, which in accordance with [39] is extremely active for CO oxidation. The size effect of catalytic activity for Ru nanoparticles within the 2–7 nm size range was correlated with the stability of the core–shell structure [44].

4 Conclusions

Ru nanoparticles were deposited on graphitic carbon nitride, N-doped carbon and mesoporous carbons. It has been shown that Ru supported on a hard-templated carbon nitride exhibited higher catalytic activity in the betulin oxidation than Ru/N-carbon composites, which can be probably attributed to a significant fraction of weak basic sites required for oxidation. Formation of betulone as the main desired reaction product (selectivity up to 27% with the yield reaching ca. 14% after 3 h) over heterogeneous Ru supported catalysts was demonstrated.

Table 2 Catalytic behaviour of Ru containing catalysts in betulin oxidation

Catalyst	X (%)	S_1 (%)	S_2 (%)	S_3 (%)	S_4 (%)	S_5 (%)	Y_1 (%)
Ru–C_3N_4–1	82.6	9.8	1.2	2.8	1.3	4.0	8.1
Ru–C_3N_4–2	72.9	7.2	0	2.7	3.6	8.9	5.3
Ru–C_3N_4–MCF	67.3	23.4	8.5	4.4	8.6	1.5	12.8
Ru–C_M	30.7	27.4	0.9	4.4	6.0	3.6	8.4
Ru–CNF	6.7	33.3	4.2	0.1	12.8	0	2.2
Ru-Sib-Imp	39.4	19.5	9.4	1.0	14.9	4.1	7.7

X conversion of betulin after 4 h (%), S_1 selectivity to betulone (%), S_2 selectivity to betulonic aldehyde (%), S_3 selectivity to betulonic acid (%), S_4 selectivity to betulinic aldehyde (%), S_5 selectivity to betulinic acid (%), Y_1 (%) yield of betulone (%)

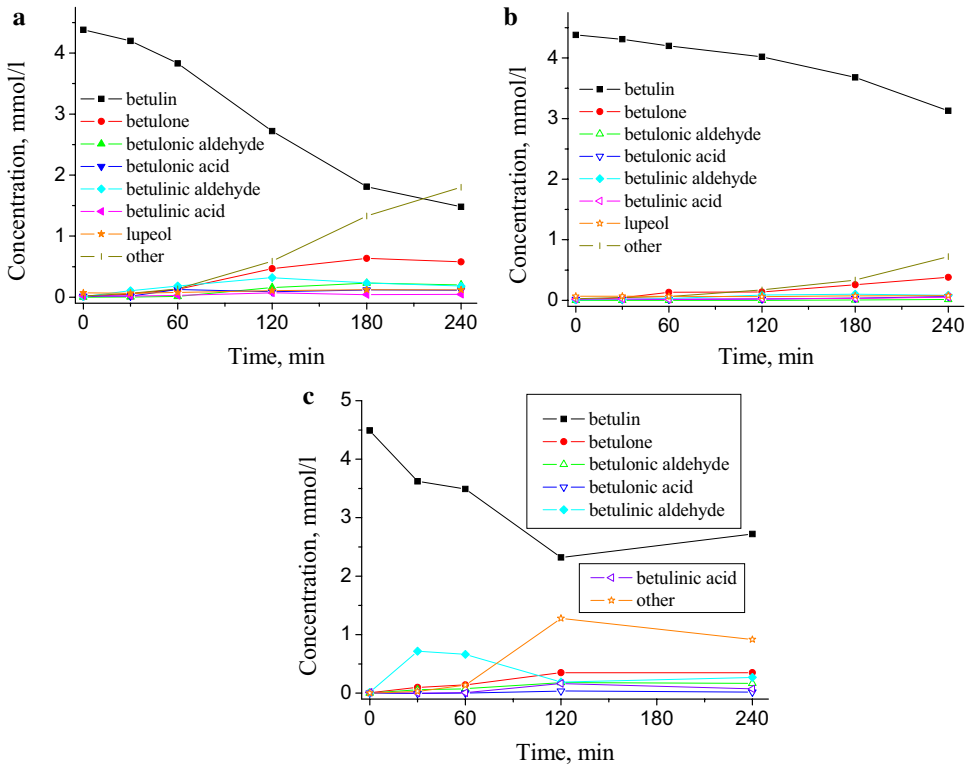

Fig. 7 Kinetics of betulin oxidation over Ru–C_3N_4–MCF (**a**), Ru–C_M (**b**) and Ru-Sib-Imp (**c**)

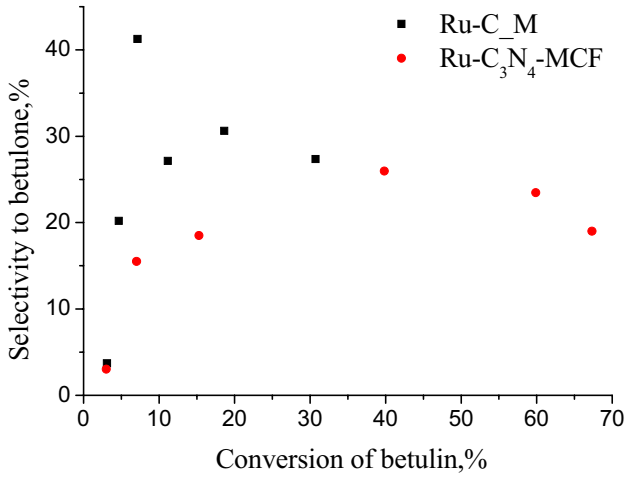

Fig. 8 Selectivity towards betulone as a function of betulin conversion

Acknowledgements Open access funding provided by Abo Akademi University (ABO). This work is part of the activities at the Johan Gadolin Process Chemistry Centre, a centre of excellence in scientific research financed by Åbo Akademi University. S. Sergienko acknowledges support from the Ministry of Education and Science of the Russian Federation (Increase Competitiveness Program of NUST "MISiS" No. K2-2018-013). The publication contains the results of studies conducted by President's of Ukraine grant for competitive projects (2017; Physicochemical bases of creation of new nanoporous and composite materials based on carbon nitride—catalysts for synthesis of biologically active substances for pharmaceutics) of the State Foundation for Fundamental Research.

Compliance with Ethical Standards

Conflict of interest The authors declare no conflict of interest.

OpenAccess This article is distributed under the terms of the Creative Commons Attribution 4.0 International License (http://creativecommons.org/licenses/by/4.0/), which permits unrestricted use, distribution, and reproduction in any medium, provided you give appropriate credit to the original author(s) and the source, provide a link to the Creative Commons license, and indicate if changes were made.

References

1. Liu H, Lei XL, Li N, Zong MH (2013) J Mol Catal B Enzym 88:32
2. Dzubak P, Hajduch M, Vydra D, Hustova A, Kvasnica M, Biedermann D, Markova L, Urban M, Sarek J (2006) Nat Prod Rep 23:394
3. Alakurtti S, Mäkelä T, Koskimies S, Yli-Kauhaluoma J (2006) Eur J Pharm Sci 29:1
4. Eckerman Ch (1985) Paperi ja Puu 3:100
5. Mäki-Arvela P, Barsukova M, Winberg I, Smeds A, Hemming J, Eränen K, Torozova A, Aho A, Volcho K, Murzin DY (2016) Chem Sel 1:3866
6. Mukharjee R, Kumar V, Srivastava SK, Agarval SK, Burman AC (2006) Med Chem 6:271
7. Tolstikova TG, Sorokina IV, Tolstikov GA, Tolstikov AG, Fletcher OB (2006) J Bioorg Chem 32:37

8. Haque S, Nawrot DA, Alakurtti S, Ghemtio L, Yli-Kauhaluoma J (2014) PLoS ONE 9:e102696
9. Chung PY, Chung LY, Navaratham P (2013) Res Microbiol 164:319
10. Motteran L, Pilone MS, Molla G, Ghisla S, Pollegioni L (2001) J Biolog Chem 276:18024
11. Das Gupta TK, Pezzuto JM (1997) Pat US 5658947
12. Baltina LA, Flekhter OB, Nigmatullina LR, Boreko EI, Pavlova NI, Nikolaeva SN, Savinova OV, Tolstikov GA (2003) Bioorg Med Chem 13:3549
13. Kogai TI, Kuznetsov BN (2008) Pat RU 2333916
14. Kim DS, Chen Z, Nguyen VT, Pezzuto JM, Qiu S, Lu ZZ (1997) Synth Commun 27:1607
15. Pezzuto JM, Darrick Kim SHL (1998) Pat US 5804575
16. Roshchin VI, Shabanova NYu, Vedernikov DN (2002) Pat RU 2190622
17. Levdansky VA, Polezhaeva NI, Kuznetsov BN (2006) Pat RU 2269541
18. Pichette A, Liu H, Roy C, Tanguay S, Simard F, Lavoie S (2004) Synth Commun 34:3925
19. Komissarova NG, Belenkova NG, Spirikhin LV, Shitikova OV, Yunusov MS (2002) Chem Nat Compd 38:58
20. Csuk R, Schmuck K, Schäfer R (2006) Tetrahedron Lett 47:8769
21. Tulisalo J, Wickholm N, Pirttimaa M, Alakurtti S, Yli-Kauhaluoma J, WO/2013/038312 (Stora Enso Oyj, Helsinki, Finland, 2013)
22. Fuchino H, Satoh T, Hida J, Terada M, Tanaka N (1998) Chem Pharm Bull 46:1051
23. Kim DK, Nam IIY, Kim JW, Shin TY, Lim JP (2002) Arch Pharm Res 25:617
24. Hata K, Hori K, Takahashi S (2002) J Nat Prod 65:645
25. Mutai C, Abatis D, Vagias C, Moreau D, Roussakis C, Roussis V (2004) Phytochemistry 65:1159
26. Dehaen W, Mashentseva AA, Seitembetov TS (2011) Molecules 16:2443
27. Zhu J, Xiao P, Li H, Carabineiro SA (2014) ACS Appl Mater Interfaces 6:16449
28. Fan Y, Li X, He X, Zeng C, Fan G, Liu Q, Tang D (2014) Int J Hydrogen Energy 39:19982
29. Kim M, Hwang S, Yu JS (2007) J Mater Chem 17:1656
30. Lin B, Wang R, Lin J, Du S, Yu X, Wei K (2007) Catal Commun 8:1838
31. Simakova IL, Demidova YS, Gläsel J, Murzina EV, Schubert T, Prosvirin IP, Etzold BJM, Murzin DY (2016) Catal Sci Technol 6:8490
32. Delidovich IV, Taran OP, Matvienko LG, Simonov AN, Simakova IL, Bobrovskaya AN, Parmon VN (2010) Catal Lett 140:14
33. Gregg SG, Sing KSW (1982) Adsorption, surface area and porosity. Academic Press, New York
34. Barrett EP, Joyner LG, Halenda PP (1951) J Am Chem Soc 73:373
35. Horvath G, Kawazoe K (1983) J Chem Eng Jpn 16:470
36. Eckerman C, Ekman R (1985) Paperi ja Puu 67:100
37. Harold PK, Leroy EA (1974) X-ray diffraction procedures: for polycrystalline and amorphous materials. Wiley, New York
38. Datta KKR, Reddy BV, Ariga K, Vinu A (2010) Angew Chem Int Ed 49:5961
39. Qadir K, Joo SH, Mun BS, Butcher DR, Renzas JR, Aksoy F, Liu Zh, Somorjai GA, Park JY (2012) Nano Lett 12:5761
40. Chakroune N, Viau G, Ammar S, Poul L, Veautier D, Chehimi MM, Mangeney C, Villain F, Fiévet F (2005) Langmuir 21:6788
41. Aho A, Roggan S, Simakova O, Salmi T, Murzin DYu (2015) Catal Today 241:195
42. Aho A, Roggan S, Eränen K, Salmi T, Murzin DYu (2015) Catal Sci Technol 5:953
43. Long B, Lin J, Wang X (2014) J Mater Chem A 2:2942
44. Joo SH, Park JY, Renzas JR, Butcher DR, Huang WY, Somorjai GA (2010) Nano Lett 10:2709

Publisher's Note Springer Nature remains neutral with regard to jurisdictional claims in published maps and institutional affiliations.